Computers and Mathematics with Applications 71 (2016) 2272–2284

Contents lists available at ScienceDirect

Computers and Mathematics with Applications

journal homepage: www.elsevier.com/locate/camwa

A fuzzy edge-weighted centroidal Voronoi tessellation model for image segmentation☆

Xiaochuan Fan [a], Lili Ju [b,*], Xiaoqiang Wang [c], Song Wang [a]

[a] Department of Computer Science and Engineering, University of South Carolina, Columbia, SC, 29208, USA
[b] Department of Mathematics, University of South Carolina, Columbia, SC 29208, USA
[c] Department of Scientific Computing, Florida State University, Tallahassee, FL 32306, USA

ARTICLE INFO

Article history:
Available online 28 November 2015

This paper is dedicated to Professor Max Gunzburger on the occasion of his 70th birthday

Keywords:
Edge-weighted centroidal Voronoi tessellation
Fuzzy clustering
Image segmentation

ABSTRACT

The centroidal Voronoi tessellation (CVT) is a special Voronoi tessellation whose generators are also the centers of mass of the corresponding Voronoi regions. The edge-weighted centroidal Voronoi tessellation (EWCVT) greatly improves the classic CVT model by adding an edge energy term in the energy functional, and has been proven to be very effective and efficient for image segmentation. In this paper, we propose a *fuzzy* edge-weighted centroidal Voronoi tessellation (FEWCVT) model which generalizes the EWCVT clustering with fuzzy membership information. The FEWCVT model novelly introduces an edge energy based on fuzzy clustering and naturally combines it into the EWCVT model, and thus appropriately combines the image intensity information with the length of cluster boundaries in a fuzzy form. In its simplest form, FEWCVT model reduces to the classic EWCVT model. An iterative algorithm is proposed for the FEWCVT model based on energy minimization. In the experiments, we apply the FEWCVT method to segment various types of images and also compare it with several existing fuzzy clustering methods to demonstrate its performance.

1. Introduction

Image segmentation is one of the oldest and most widely studied problems in computer vision and image processing. Its goal is to change the representation of an image to something that is more meaningful and more convenient to analyze [1], although it is quite difficult to define "meaningful" precisely and quantitatively. Specifically, image segmentation is used to divide an image into a number of non-overlapping regions, which share some characteristics, e.g. color, brightness, texture, boundary continuity, etc. Many algorithms have been proposed to solve this problem, however, image segmentation is still a very challenging research topic, due to the huge varieties of images in the real world.

Clustering, as a powerful tool for retrieving generic structural information from a large set of data, has been proved very effective for image segmentation. Generally clustering is a process of classifying a large number of data samples into smaller data groups with maximum homogeneity [2]. By taking each pixel as a data point, a clustering algorithm can group all the pixels in an image into a small number of clusters and generates an image segmentation. There are two categories of clustering methods: hard clustering and fuzzy clustering. The main difference between them is that while in hard clustering

☆ This work was partially supported by the US AFOSR grant FA9550-11-1-0327 and the US NSF grant IIS-1017199, and by the Open Project Program grant A1420 of the State Key Lab of CAD & CG in Zhejiang University, China.
* Corresponding author.
E-mail addresses: fan23@email.sc.edu (X. Fan), ju@math.sc.edu (L. Ju), wwang3@fsu.edu (X. Wang), songwang@cec.sc.edu (S. Wang).

http://dx.doi.org/10.1016/j.camwa.2015.11.003
0898-1221/

a single data sample can only belong to one cluster, in fuzzy clustering a data sample is allowed to belong to multiple clusters with different degrees of membership [3]. Because fuzzy clustering can retain more image information than hard clustering in some situations, it has been extensively researched and applied in image segmentation.

Among existing fuzzy clustering algorithms, the most well-known method is the fuzzy c-means (FCM) [4]. When using FCM for image segmentation, it works well on images with homogeneous regions. However, because it only considers the pixel intensity information, but not the pixel spatial contextual information, FCM-based image segmentation is usually sensitive to image noises. To solve the limitations of the conventional FCM algorithm, many modified FCM algorithms have been proposed by exploiting local spatial information from the original image. Two strategies are usually used to incorporate such local spatial information—*image smoothing* and *regularization*.

For the image-smoothing strategy, a new image is constructed by applying smoothing filters to the original image and then FCM clustering is performed on this filtered image [5,6]. Szilagyi et al. [5] proposed an enhanced FCM (EnFCM) algorithm, where a linearly weighted sum image is formed from both the original image and the smoothly filtered image. Cai et al. [6] proposed a fast generalized FCM (FGFCM) algorithm, based on a new local similarity measure that incorporates both the local spatial and intensity information to form a non-linearly weighted sum image. Two variants of the FGFCM, the FGFCM_S1 and the FGFCM_S2, are further presented in [6] by modifying the similarity measure. Using the image-smoothing strategy, the filtered image naturally incorporates the local spatial information and the image noise can be removed to some extent before image segmentation. However, important structural boundaries may get blurred, resulting in inaccurate or even incorrect image segmentations. Besides, in order to reduce the computation burden, EnFCM and FGFCM perform the clustering on the image histogram instead of image pixels. This makes it impossible to further utilize local spatial information in image segmentation.

For the regularization strategy, the FCM objective function is modified [7–9] by introducing a regularization term which allows the clustering of a pixel to be influenced by the pixels in its local neighborhood. Ahmed et al. [7] added a spatial-neighbors term to the objective function of FCM as a regularizer, which leads to an FCM_S algorithm. The computational cost of FCM_S is high since the spatial-neighbors term has to be recalculated in every clustering iteration. To address this issue, Chen and Zhang [8] proposed FCM_S1 and FCM_S2, two variants of the FCM_S algorithm, by combining both the image-smoothing strategy and the regularization strategy. In FCM_S1 and FCM_S2, mean or median filters are applied to the original image to form a filtered image in advance and the pixel intensity at the filtered image is then taken to define the regularization term. More recently, Stelios et al. [9] proposed a fuzzy local information c-means clustering algorithm (FLICM), in which the membership values of the pixels in the neighborhood are also incorporated in the regularization term. Different from the previous fuzzy c-means algorithms, FLICM is completely free of any parameter determination. While the regularization strategy can deal with image noises effectively, these above-mentioned algorithms either only put their focus on the local spatial clustering coherence or are designed empirically, lacking exact meaning of the regularization terms.

Boundary length (or area in 3D space) has been widely used as a regularity term for image segmentation. In the classic Chan–Vese model [10–12], an evolving curve (cluster boundary) length penalty term is used to control the smoothness of the zero level set and improve the robustness against image noise. More recently, an edge-weighted centroidal Voronoi tessellation (EWCVT) model was proposed by Wang et al. [13], which works well on sophisticated image segmentation and is very flexible to handle any number of clusters [14–17]. In EWCVT, a new edge-related energy term, which is proven to be proportional to the length of the cluster boundary, is added to the classic centroidal Voronoi tessellations (CVT) model [18–23], which is a special type of Voronoi tessellation whose generators are also the centers of mass (centroids) of the Voronoi regions. With the new edge energy term, EWCVT can effectively control the smoothness of the resulting segmentation boundaries and achieve good robustness to image noises with high computational efficiency.

In this paper, we first propose a novel fuzzy edge-weighted centroidal Voronoi tessellations (FEWCVT) model, and then develop and analyze corresponding algorithms for image segmentation based on energy minimization. The energy functional in the new model consists of two parts, one is the fuzzy clustering energy which is almost equivalent to the objective function of the standard FCM algorithm, and the other is the fuzzy edge energy. FEWCVT inherits the desirable advantages of EWCVT such as the robustness to the image noises and the ability to handle any number of clusters. Furthermore, FEWCVT has the merits of fuzzy clustering algorithms by generating essentially a soft clustering and segmentation result.

The remainder of this paper is organized as follows. In Section 2, we will first review the classic CVT and EWCVT models for image segmentation. The new fuzzy edge-weighted centroidal Voronoi tessellation model is proposed in Section 3 and a computing algorithm is then developed and analyzed in detail in Section 4. The experimental results, together with qualitative and quantitative comparisons against several existing popular fuzzy clustering algorithms are reported in Section 5, followed by concluding remarks in Section 6.

2. CVT and EWCVT for image segmentation

A digital image can be regarded as a function f defined on a domain $\Omega \subseteq \mathbb{R}^N$ in the Euclidean space where the values of f represent the color or intensity values of a set of pixels D. In this paper, the 2D rectangular image will be considered, i.e., $\Omega \subseteq \mathbb{R}^2$. We note that the proposed algorithm can be easily applied to higher dimensional and non-rectangular images. In the 2D case, pixels are usually denoted by their coordinates which are positive integers, thus elements in D are in fact integer pairs. For simplicity, we use bold lowercase letters, like $\mathbf{p}$, $\mathbf{q}$, etc., to denote these pixels.

2.1. CVT and clustering energy

Let $\mathbb{U} = \{f(\mathbf{p})\}_{\mathbf{p}\in D}$ denote the set of intensity/color values of the image over D and $\mathcal{W} = \{w_l\}_{l=1}^{L}$ a set of typical colors (or intensity values). The *Voronoi* region V_k in $\mathbb{U}$ corresponding to the color w_k is defined by

$$V_k = \left\{f(\mathbf{p}) \in \mathbb{U} \;\middle|\; |f(\mathbf{p}) - w_k| \le |f(\mathbf{p}) - w_l|\,,\ \text{for } l = 1, \ldots, L,\ l \ne k\right\}, \quad k = 1, \ldots, L \tag{1}$$

where $|\cdot|$ is some predefined metric measure such as the Euclidean distance. The set $\mathcal{V} = \{V_l\}_{l=1}^{L}$ is called a *Voronoi tessellation* or *Voronoi clustering* of the set $\mathbb{U}$. The set of chosen intensities $\mathcal{W} = \{w_l\}_{l=1}^{L}$ are referred as the *Voronoi generators*. Since we have $\mathring{V}_i \cap \mathring{V}_j = \emptyset$ if $i \ne j$ and $\mathbb{U} = \cup_{l=1}^{L} V_l$, the Voronoi tessellation $\mathcal{V}$ can be viewed as a special partition of $\mathbb{U}$. Given a partition of $\mathbb{U}$, denoted by $\{U_l\}_{l=1}^{L}$, the *centroid* (i.e. *center of mass* or *cluster mean*) of each cell U_l is defined to be the intensity $\bar{w}_l \in U_l$ such that

$$\bar{w}_l = \arg\min_{w\in U_l} \sum_{f(\mathbf{p})\in U_l} |f(\mathbf{p}) - w|^2\,. \tag{2}$$

For an arbitrary Voronoi tessellation $(\{w_l\}_{l=1}^{L};\ \{V_l\}_{l=1}^{L})$ of $\mathbb{U}$, it is often the case that $w_l \ne \bar{w}_l$ for $l = 1, 2, \ldots, L$, where $\{\bar{w}_l\}_{l=1}^{L}$ are the corresponding centroids of $\{V_l\}_{l=1}^{L}$. If the generators of the Voronoi regions $\{V_l\}_{l=1}^{L}$ of $\mathbb{U}$ coincide with their corresponding centroids, i.e., $w_l = \bar{w}_l$ for $l = 1, 2, \ldots, L$, then we call the Voronoi tessellation $\{V_l\}_{l=1}^{L}$ a *centroidal Voronoi tessellation* (CVT) of $\mathbb{U}$ and refer to $\{w_l\}_{l=1}^{L}$ as the corresponding CVT generators.

The construction of CVTs often can be achieved by an "energy" minimization process. Generally, for any set of points $\mathcal{W} = \{w_l\}_{l=1}^{L}$ and any partition $\mathcal{U} = \{U_l\}_{l=1}^{L}$ of $\mathbb{U}$, let us define the classic *clustering energy* of $(\mathcal{W};\ \mathcal{U})$ as follows:

$$E_C(\mathcal{W};\ \mathcal{U}) = \sum_{l=1}^{L} \sum_{f(\mathbf{p})\in U_l} |f(\mathbf{p}) - w_l|^2\,. \tag{3}$$

Suppose that we have determined the clusters $\{U_l\}_{l=1}^{L}$ for a given 2D digital image represented in color space by $f(\mathbf{p})$ for $\mathbf{p} \in D$. Then a segmentation in the physical space of the image can be naturally produced as $\mathcal{D} = \{D_l\}_{l=1}^{L}$ where $D_l = \{\mathbf{p} \in D \mid f(\mathbf{p}) \in U_l\}$. Consequently, the classic clustering energy (3) can be rewritten in physical segmentation terminology as

$$E_C(\mathcal{W};\ \mathcal{D}) = \sum_{l=1}^{L} \sum_{\mathbf{p}\in D_l} |f(\mathbf{p}) - w_l|^2\,. \tag{4}$$

Obviously, D_l can be also written in another form as $D_l = \{\mathbf{p} \in D \mid \mu_l(\mathbf{p}) = 1\}$ where $\mu_l(\mathbf{p}) : D \to \{0, 1\}$ indicates whether $f(\mathbf{p}) \in U_l$. Thus we also have

$$E_C(\mathcal{W};\ \mathcal{D}) = \sum_{l=1}^{L} \sum_{\mathbf{p}\in D} \mu_l(\mathbf{p})\, |f(\mathbf{p}) - w_l|^2\,. \tag{5}$$

Then $E_C(\mathcal{W};\ \mathcal{D})$ is minimized only if $(\mathcal{W};\ \mathcal{D})$ forms a CVT of D, i.e. $\mathcal{D}$ are Voronoi regions of D associated with the generators $\mathcal{W}$ and simultaneously $\mathcal{W}$ are the corresponding centroids of the region $\mathcal{D}$. Some typical clustering energy minimization methods can be found in [24–26].

2.2. Edge energy and EWCVT

Wang et al. [13] proposed a generalization of the classic CVT model, the EWCVT model, which adds an edge related energy term $E_{\mathcal{L}}$ to the CVT energy function to enforce the spatial continuity and smoothness on the cluster boundary. The energy function of EWCVT can be written as

$$E(\mathcal{W};\ \mathcal{D}) = E_C(\mathcal{W};\ \mathcal{D}) + \lambda E_{\mathcal{L}}(\mathcal{D})\,, \tag{6}$$

where, λ is the weighting parameter to balance these two energy terms.

For each pixel $\mathbf{p} \in D$, denote $\mathbb{N}_\omega(\mathbf{p})$ a local neighborhood of $\mathbf{p}$, which can be a $\omega \times \omega$ square centered at $\mathbf{p}$ or a disk centered at $\mathbf{p}$ with radius ω. Any pixel $\mathbf{q} \in \mathbb{N}_\omega(\mathbf{p})$ is called a neighbor pixel of $\mathbf{p}$. We then define a local characteristic function $\chi_{\mathbf{p}} : \mathbb{N}_\omega(\mathbf{p}) \to \{0, 1\}$ as

$$\chi_{\mathbf{p}}(\mathbf{q}) = \begin{cases} 1 & \text{if } \pi_{\mathcal{U}}(\mathbf{q}) \ne \pi_{\mathcal{U}}(\mathbf{p}) \\ 0 & \text{otherwise,} \end{cases} \tag{7}$$

where $\pi_{\mathcal{U}}(\mathbf{p}) : D \to \{1, \ldots, L\}$ indicates the index of the cluster that $\mathbf{p}$ belongs to. Then, the edge energy for each $\mathbf{p} \in D$ can be defined as

$$\varepsilon_{\mathcal{L}}(\mathbf{p}) = \sum_{\mathbf{q} \in \mathbb{N}_{\omega}(\mathbf{p})} \chi_{\mathbf{p}}(\mathbf{q}).$$

Naturally, the total edge energy of an image is the summation of $\varepsilon_{\mathcal{L}}(\mathbf{p})$ over D

$$E_{\mathcal{L}}(\mathcal{D}) = \sum_{\mathbf{p} \in D} \varepsilon_{\mathcal{L}}(\mathbf{p}) = \sum_{\mathbf{p} \in D} \sum_{\mathbf{q} \in \mathbb{N}_{\omega}(\mathbf{p})} \chi_{\mathbf{p}}(\mathbf{q}). \tag{8}$$

Note that $E_{\mathcal{L}}$ only depends on the segmentation/partition $\mathcal{D}$. The proof of the proportional relation between the edge energy and the boundary length can be found in [13]. More specifically, $E_{\mathcal{L}}$ is proportional to $\omega^3 H$ in the asymptotic sense where H is the length of boundary. The use of edge energy naturally indicates that the cluster boundary which minimizes the overall energy function should be as short as possible. As a result, the smoothness of the resulting boundaries can be effectively controlled and the robustness to noises is improved significantly.

3. Fuzzy edge-weighted centroidal Voronoi tessellations

Fuzzy logic is widely used in data clustering. In many situations, fuzzy clustering methods can achieve better segmentation result than hard clustering. In this section we will develop a Fuzzy Edge-Weighted Centroidal Voronoi Tessellation model for image segmentation, in which both the classic clustering energy and the edge energy based on the boundary length are generalized to a fuzzy form. In addition, the clustering algorithm for the FEWCVT model based on the Newton–Raphson optimization method will also be discussed and analyzed.

3.1. Fuzzy clustering energy and fuzzy edge energy

Let $\mu_l(\mathbf{p})$ be a membership function which represents the degree of membership of the pixel $\mathbf{p}$ in the lth cluster satisfying

$$\mu_l(\mathbf{p}) \in [0, 1] \quad \text{and} \quad \sum_{l=1}^{L} \mu_l(\mathbf{p}) = 1, \quad \forall \mathbf{p} \in D,$$

and set $\mathcal{D}^{fuzzy} = \{D_l^{fuzzy}\}_{l=1}^{L}$ which denotes a fuzzy segmentation in the physical space of the image where

$$D_l^{fuzzy} = \{\mu_l(\mathbf{p}) \mid \mathbf{p} \in D\}. \tag{9}$$

Note that (10) can reduce to (5) when $\mu_l(\mathbf{p}) \in \{0, 1\}$, i.e., $\mu_l(\mathbf{p})$ only takes value 0 or 1.

Then we can naturally define the fuzzy clustering energy as

$$E_C^{fuzzy}\left(\mathcal{W}; \mathcal{D}^{fuzzy}\right) = \sum_{\mathbf{p} \in D} \sum_{l=1}^{L} \mu_l^m(\mathbf{p}) \left|f(\mathbf{p}) - w_l\right|^2, \tag{10}$$

where $m > 1$ is a weighting exponent on each fuzzy membership and determines the amount of fuzziness of the resulting classification. Next we need define the fuzzy edge energy for a given cluster. Let us revisit the definition of *edges* in the context of fuzzy clustering. For the fuzzy clustering, crisp boundary no longer exists, since each pixel $\mathbf{p} \in D$ belongs to all segments to some degree. In other words, every $\mathbf{p}$ is the boundary point to some degree. Thus, different from [13] in which the edge energy is defined as the sum of the number of edge points within a neighborhood, we generally define the *fuzzy edge energy* as the sum of the membership of each pixel within a neighborhood.

For each $\mathbf{p} \in D$, we first define the fuzzy local characteristic function $\chi_{\mathbf{p}}^{fuzzy} : \mathbb{N}_{\omega}(\mathbf{p}) \to [0, 1]$ for neighbor points $\mathbf{q}$ of $\mathbf{p}$ as

$$\chi_{\mathbf{p}}^{fuzzy}(\mathbf{q}) = \sum_{l=1}^{L} \mu_l(\mathbf{p})\left(1 - \mu_l(\mathbf{q})\right). \tag{11}$$

According to the definition of the membership function, $(1 - \mu_l(\mathbf{q}))$ can be regarded as the degree of membership that $\mathbf{q}$ does not belong to the lth cluster. Thus $\chi_{\mathbf{p}}(\mathbf{q})$ actually represents the degree that $\mathbf{p}$ and its neighbor $\mathbf{q}$ belong to different clusters. We name such a degree as a *local fuzzy edge* with regards to $\mathbf{p}$. It can be easily seen that the local characteristic function defined in (11) can reduce to (7) when $\mu_l(\mathbf{p}) \in \{0, 1\}$.

We then define the local fuzzy edge energy for pixel $\mathbf{p}$ to be the average of the membership values of the pixels in $\mathbb{N}_{\omega}(\mathbf{p})$, i.e.,

$$\varepsilon_{\mathcal{L}}^{fuzzy}(\mathbf{p}) = \frac{1}{|\mathbb{N}_{\omega}|} \sum_{\mathbf{q} \in \mathbb{N}_{\omega}(\mathbf{p})} \chi_{\mathbf{p}}^{fuzzy}(\mathbf{q}), \tag{12}$$

where $|\mathbb{N}_\omega|$ is the cardinality of $\mathbb{N}_\omega(\mathbf{p})$. Naturally, the total fuzzy edge energy is the summation of $\varepsilon_{\mathcal{L}}(\mathbf{p})$ over D as

$$E_{\mathcal{L}}^{fuzzy}\left(\mathcal{D}^{fuzzy}\right) = \sum_{\mathbf{p}\in D} \varepsilon_{\mathcal{L}}^{fuzzy}(\mathbf{p}). \tag{13}$$

Note that the fuzzy edge energy only depends on the segmentation $\mathcal{D}^{fuzzy}$.

3.2. Fuzzy edge-weighted clustering energy and FEWCVT

Combining together the fuzzy edge energy $E_{\mathcal{L}}^{fuzzy}$ (13) with the classical fuzzy clustering energy E_C^{fuzzy} (10), we define the *fuzzy edge-weighted clustering energy* as follows

$$\begin{aligned} E^{fuzzy}\left(\mathcal{W};\mathcal{D}^{fuzzy}\right) &= E_C^{fuzzy}\left(\mathcal{W};\mathcal{D}^{fuzzy}\right) + \lambda E_{\mathcal{L}}^{fuzzy}\left(D^{fuzzy}\right) \\ &= \sum_{\mathbf{p}\in D}\left[\varepsilon_C^{fuzzy}(\mathbf{p}) + \lambda\varepsilon_{\mathcal{L}}^{fuzzy}(\mathbf{p})\right] \\ &= \sum_{\mathbf{p}\in D}\sum_{l=1}^{L}\mu_l^m(\mathbf{p})\,|f(\mathbf{p}) - w_l|^2 + \frac{\lambda}{|\mathbb{N}_\omega|}\sum_{\mathbf{p}\in D}\sum_{l=1}^{L}\mu_l(\mathbf{p})\sum_{\mathbf{q}\in\mathbb{N}_\omega(\mathbf{p})}(1-\mu_l(\mathbf{q})) \end{aligned} \tag{14}$$

where λ is a positive weighting factor to control the balance between the fuzzy clustering energy and the fuzzy edge energy. The second term in (14), the fuzzy edge energy, is to act as a regularizer of the segmentation.

Definition 1. We call $(\hat{\mathcal{W}};\hat{\mathcal{D}}^{fuzzy})$ a *fuzzy edge-weighted centroidal Voronoi tessellation* (FEWCVT) of D if and only if

$$(\hat{\mathcal{W}};\hat{\mathcal{D}}^{fuzzy}) \in \arg\min_{(\mathcal{W};\mathcal{D}^{fuzzy})} E^{fuzzy}\left(\mathcal{W};\mathcal{D}^{fuzzy}\right), \tag{15}$$

subject to

$$\begin{cases} \sum_{l=1}^{L}\mu_l(\mathbf{p}) - 1 = 0, \\ 0 \le \mu_l(\mathbf{p}) \le 1, \quad l = 1,\ldots,L, \end{cases} \tag{16}$$

for all $\mathbf{p}\in D$,

We note here that "arg min" refers to both global and local minimizers which may not be unique for the problem. Our segmentation goal is to find such clustering $(\hat{\mathcal{W}};\hat{\mathcal{D}}^{fuzzy})$ for a given image $\mathbb{U} = \{f(\mathbf{p})\}_{\mathbf{p}\in D}$.

4. Algorithm for computing FEWCVTs

The above constrained optimization problem for the FEWCVT model can be solved using the Lagrange multiplier method with a Lloyd-type iteratively updating process between $\mathcal{W}$ and $\mathcal{D}^{fuzzy}$ based on the CVT-methodology [18,13].

Assume that $\mathcal{W}$ is fixed, we will solve for $\bar{\mathcal{D}}^{fuzzy}$ such that

$$\bar{\mathcal{D}}^{fuzzy} \in \arg\min_{\mathcal{D}^{fuzzy}} E^{fuzzy}\left(\mathcal{W};\mathcal{D}^{fuzzy}\right). \tag{17}$$

In some sense, the minimizer $\bar{\mathcal{D}}^{fuzzy}$ can be regarded as the corresponding *fuzzy edge-weighted Voronoi regions* associated with $\mathcal{W}$.

Let $\mathbf{p}$ be an arbitrary point in D. Define

$$\Lambda\left(\mu_1(\mathbf{p}),\ldots,\mu_L(\mathbf{p}),\rho\right) = \sum_{\mathbf{p}\in D}\sum_{l=1}^{L}\mu_l^m(\mathbf{p})\,d_l(\mathbf{p}) + \frac{\lambda}{|\mathbb{N}_\omega|}\sum_{\mathbf{p}\in D}\sum_{\mathbf{q}\in\mathbb{N}_\omega(\mathbf{p})}\chi_{\mathbf{p}}(\mathbf{q}) + \rho\left(\sum_{l=1}^{L}\mu_l(\mathbf{p}) - 1\right), \tag{18}$$

where $d_l(\mathbf{p}) = |f(\mathbf{p}) - w_l|^2$ and ρ is the Lagrange multiplier associated with the first constraint $\sum_{l=1}^{L}\mu_l(\mathbf{p}) - 1 = 0$. We need minimize $\Lambda\left(\mu_1(\mathbf{p}),\ldots,\mu_L(\mathbf{p})\right)$ given that $\{\{\mu_l(\mathbf{q})\}_{l=1}^{L} \mid \mathbf{q}\in D,\ \mathbf{q}\ne\mathbf{p}\}$ is fixed.

In order to obtain the derivative of Λ with respect to $\mu_l(\mathbf{p})$, let us rewrite (18) as

$$\begin{aligned} \Lambda\left(\mu_1(\mathbf{p}),\ldots,\mu_L(\mathbf{p}),\rho\right) = &\left[\sum_{\mathbf{p}'\in D\setminus\mathbf{p}}\sum_{l=1}^{L}\mu_l^m(\mathbf{p}')\,d_l(\mathbf{p}') + \sum_{l=1}^{L}\mu_l^m(\mathbf{p})\,d_l(\mathbf{p}) + \rho\left(\sum_{l=1}^{L}\mu_l(\mathbf{p}) - 1\right)\right] \\ &+ \lambda\varepsilon_{\mathcal{L}}^{fuzzy}(\mathbf{p}) + \left[\sum_{\mathbf{p}'\in D\setminus\mathbf{p}}\lambda\varepsilon_{\mathcal{L}}^{fuzzy}(\mathbf{p}')\right]. \end{aligned} \tag{19}$$

The partial derivative of the first term on the right side of (19) with respect to $\mu_l(\mathbf{p})$ is given by

$$m\mu_l^{m-1}(\mathbf{p})\, d_l(\mathbf{p}) + \rho. \tag{20}$$

The second term can be rewritten as

$$\lambda\varepsilon_{\mathcal{L}}^{fuzzy}(\mathbf{p}) = \frac{\lambda}{|\mathbb{N}_\omega|}\sum_{l=1}^{L}\left(\mu_l(\mathbf{p})(1-\mu_l(\mathbf{p})) + \mu_l(\mathbf{p})\sum_{\mathbf{q}\in\mathbb{N}_\omega(\mathbf{p})\setminus\mathbf{p}}(1-\mu_l(\mathbf{q}))\right),$$

so its partial derivative with respect to $\mu_l(\mathbf{p})$ is

$$\frac{\lambda}{|\mathbb{N}_\omega|}\left(1-2\mu_l(\mathbf{p}) + \sum_{\mathbf{q}\in\mathbb{N}_\omega(\mathbf{p})\setminus\mathbf{p}}(1-\mu_l(\mathbf{q}))\right). \tag{21}$$

Now let us consider the third term. Let us change the value of $\mu_l(\mathbf{q})$ to $\mu_l(\mathbf{q}) + \delta\mu_l(\mathbf{q})$. For each $\mathbf{p}'$ which is outside of $\mathbb{N}_\omega(\mathbf{p})$, the change of $\mu_l(\mathbf{p})$ will not affect $\varepsilon_{\mathcal{L}}^{fuzzy}(\mathbf{p}')$. On the other hand, for each $\mathbf{p}'$ inside $\mathbb{N}_\omega(\mathbf{p})$, the change of $\varepsilon_{\mathcal{L}}^{fuzzy}(\mathbf{p}')$ is

$$\frac{1}{|\mathbb{N}_\omega|}\mu_l(\mathbf{p}')(1-(\mu_l(\mathbf{p})+\delta\mu_l(\mathbf{p}))) - \frac{1}{|\mathbb{N}_\omega|}\mu_l(\mathbf{p}')(1-\mu_l(\mathbf{p})) = -\frac{\mu_l(\mathbf{p}')}{|\mathbb{N}_\omega|}\delta\mu_l(\mathbf{p}).$$

Thus, the total change of the third term is

$$-\frac{\lambda\delta\mu_l(\mathbf{p})}{|\mathbb{N}_\omega|}\sum_{\mathbf{p}'\in\mathbb{N}_\omega(\mathbf{p})\setminus\mathbf{p}}\mu_l(\mathbf{p}').$$

We then obtain the partial derivative of the third term with respect to $\mu_l(\mathbf{p})$ as

$$-\frac{\lambda}{|\mathbb{N}_\omega|}\sum_{\mathbf{p}'\in\mathbb{N}_\omega(\mathbf{p})\setminus\mathbf{p}}\mu_l(\mathbf{p}'). \tag{22}$$

Combining (20), (21), and (22), we easily obtain the partial derivative of Λ with respect to $\mu_l(\mathbf{p})$ as

$$\begin{aligned}\frac{\partial\Lambda}{\partial\mu_l(\mathbf{p})} &= m\mu_l^{m-1}(\mathbf{p})\, d_l(\mathbf{p}) + \rho - \frac{\lambda}{|\mathbb{N}_\omega|}\sum_{\mathbf{q}\in\mathbb{N}_\omega(\mathbf{p})\setminus\mathbf{p}}\mu_l(\mathbf{q}) + \frac{\lambda}{|\mathbb{N}_\omega|}\left(1-2\mu_l(\mathbf{p}) + \sum_{\mathbf{q}\in\mathbb{N}_\omega(\mathbf{p})\setminus\mathbf{p}}(1-\mu_l(\mathbf{q}))\right)\\ &= m\mu_l^{m-1}(\mathbf{p})\, d_l(\mathbf{p}) + \rho + \frac{\lambda}{|\mathbb{N}_\omega|}\left(1-2\mu_l(\mathbf{p}) + \sum_{\mathbf{q}\in\mathbb{N}_\omega(\mathbf{p})\setminus\mathbf{p}}(1-2\mu_l(\mathbf{q}))\right)\\ &= m\mu_l^{m-1}(\mathbf{p})\, d_l(\mathbf{p}) + \rho + \frac{\lambda}{|\mathbb{N}_\omega|}\left(\sum_{\mathbf{q}\in\mathbb{N}_\omega(\mathbf{p})}(1-2\mu_l(\mathbf{q}))\right).\end{aligned} \tag{23}$$

Thus, we obtain a system of $L+1$ equations for minimizing $\Lambda(\mu_1(\mathbf{p}), \ldots, \mu_L(\mathbf{p}))$ as

$$\begin{cases} m\mu_l^{m-1}(\mathbf{p})\, d_l(\mathbf{p}) + \rho + \dfrac{\lambda}{|\mathbb{N}_\omega|}\left(\displaystyle\sum_{\mathbf{q}\in\mathbb{N}_\omega(\mathbf{p})}(1-2\mu_l(\mathbf{q}))\right) = 0, \quad l = 1, 2, \ldots, L,\\ \displaystyle\sum_{l=1}^{L}\mu_l(\mathbf{p}) = 1,\end{cases} \tag{24}$$

with an additional requirement

$$0 \le \mu_l(\mathbf{p}) \le 1$$

for all $\mathbf{p} \in D$.

The above system is obviously nonlinear when $m > 1$ and $m \neq 2$. In such case the Newton–Raphson method is adopted to solve the system to find its root $\{\bar{\mu}_l(\mathbf{p})\}_{l=1}^{L}$ (the membership values) and ρ. The Jacobian Matrix of this system (24), a matrix of dimension $(L+1)\times(L+1)$, is as follows

$$J(\mathbf{p}) = \begin{bmatrix} \dfrac{m(m-1)\, d_1(\mathbf{p})}{\mu_1^{2-m}(\mathbf{p})} & 0 & \cdots & 0 & 1\\ 0 & \dfrac{m(m-1)\, d_2(\mathbf{p})}{\mu_2^{2-m}(\mathbf{p})} & \ddots & \vdots & 1\\ \vdots & \ddots & \ddots & 0 & 1\\ 0 & \cdots & 0 & \dfrac{m(m-1)\, d_L(\mathbf{p})}{\mu_L^{2-m}(\mathbf{p})} & 1\\ 1 & 1 & \cdots & 1 & 0 \end{bmatrix}. \tag{25}$$

The starting value for the $(L+1)$ unknowns are specified according to the initial clustering configuration or the result of the last Newton–Raphson iteration. The Newton–Raphson iterations proceed until the values of the unknowns in successive iterations converge to a pre-set level of tolerance or the number of iterations exceeds a maximum.

Remark 1. When $m=2$, the system (24) is linear, then the Newton–Raphson method converges in one step and the solution has a closed form as shown below. Solving (24) with $m=2$ for $\bar{\mu}_l(\mathbf{p})$, we get

$$\bar{\mu}_l(\mathbf{p}) = -\frac{\frac{\lambda}{|\mathbb{N}_\omega|}\left(\sum_{\mathbf{q}\in\mathbb{N}_\omega(\mathbf{p})}(1-2\mu_l(\mathbf{q}))\right)+\rho}{2d_l(\mathbf{p})}. \tag{26}$$

Since $\sum_{l=1}^{L}\mu_l(\mathbf{p})=1$, it holds

$$\sum_{k=1}^{L}\frac{\frac{\lambda}{|\mathbb{N}_\omega|}\left(\sum_{\mathbf{q}\in\mathbb{N}_\omega(\mathbf{p})}(1-2\mu_k(\mathbf{q}))\right)+\rho}{2d_k(\mathbf{p})} = -1, \tag{27}$$

which deduces

$$\rho = -\frac{1+\sum_{k=1}^{L}\frac{\frac{\lambda}{|\mathbb{N}_\omega|}\left(\sum_{\mathbf{q}\in\mathbb{N}_\omega(\mathbf{p})}(1-2\mu_k(\mathbf{q}))\right)}{2d_k(\mathbf{p})}}{\sum_{k=1}^{L}\frac{1}{2d_k(\mathbf{p})}}. \tag{28}$$

Substituting it into (26), the zero-gradient condition for the membership estimator indicates

$$\bar{\mu}_l(\mathbf{p}) = \frac{1+\frac{\lambda}{|\mathbb{N}_\omega|}\sum_{k=1}^{L}\left(\frac{\sum_{\mathbf{q}\in\mathbb{N}_\omega(\mathbf{p})}(\mu_k(\mathbf{q})-\mu_l(\mathbf{q}))}{d_l(\mathbf{p})}\right)}{d_l(\mathbf{p})\sum_{k=1}^{L}\frac{1}{d_k(\mathbf{p})}} \tag{29}$$

for $l=1,2,\ldots,L$.

Remark 2. We also specially note that the memberships $\{\bar{\mu}_l(\mathbf{p})\}_{l=1}^{L}$ obtained during each iteration may not lie exactly in $[0,1]$, i.e., violate the constraint $0\le\mu_l(\mathbf{p})\le 1$. If this occurs, in the current implementation we simply set the violated memberships to either 0 and 1 (depending on which one is closer), and then normalize the whole memberships to make the sum equal to 1. This approach has worked fine for all tested examples in numerical experiments although the energy decreasing property could be violated during the optimization iterations. For future investigation, it would be particularly interesting to incorporate the projected gradient descent method [27] into the proposed FEWCVT model, that can derive the projection of the memberships $\{\bar{\mu}_l(\mathbf{p})\}_{l=1}^{L}$ onto the probability simplex [28]. By using this projection technique, one could guarantee the energy decreasing property and further improve the performance of the model.

Next assume that $\mathcal{D}^{fuzzy}$ is fixed, we need solve $\bar{\mathcal{W}}$ such that

$$\bar{\mathcal{W}} = \arg\min_{\mathcal{W}} E^{fuzzy}\left(\mathcal{W};\mathcal{D}^{fuzzy}\right). \tag{30}$$

In some sense, such minimizer $\bar{\mathcal{W}}$ can be regarded as the corresponding *centroids* associated with $\mathcal{D}^{fuzzy}$. Since the fuzzy edge energy term does not depend on $\mathcal{W}$, this task is easy to do. Taking the partial derivative of $E^{fuzzy}\left(\mathcal{W};\mathcal{D}^{fuzzy}\right)$ with respect to $\mathcal{W}$, and setting the result to zero, we can get

$$\bar{w}_l = \frac{\sum_{\mathbf{p}\in D}\mu_l^m(\mathbf{p})f(\mathbf{p})}{\sum_{\mathbf{p}\in D}\mu_l^m(\mathbf{p})}, \quad l=1,2,\ldots,L. \tag{31}$$

Now we propose a FEWCVT Algorithm for image segmentation as follows:

Note that in the above FEWCVT algorithm the de-fuzzification is the process of interpreting the membership degrees into crisp partition. Here, we use a simple method which assigns the point $\mathbf{p}$ to the cluster with the largest membership value. When $m=2$, it is easy to show that the overall complexity of FEWCVT algorithm is $O(\omega^2\times L^2\times\#(\text{pixels}))$ per iteration.

Convergence of this FEWCVT algorithm can be obtained straightly from the following energy decreasing property.

Algorithm-FEWCVT

1. Pre-select a set of generators $\{w_l\}_{l=1}^L$ and an initial partition $\{D_l^{fuzzy}\}_{l=1}^L$ of the physical space D (can be arbitrarily chosen).
2. **for all** pixels $\mathbf{p} \in D$ do
   Solve (24) to determine $\{\bar{\mu}_l(\mathbf{p})\}_{l=1}^L$ and take them as the new membership values.
   end for
3. Calculate $\{\bar{w}_l\}_{l=1}^L$ using (31) and take them as the new generators.
4. If no membership of the points in the loop is changed, return $\{D_l^{fuzzy}\}_{l=1}^L$ and exit; otherwise, go to Step 2.
5. De-fuzzification if needed.

Theorem 1. *Let* $\{\mathcal{W}_{(n)}, \mathcal{D}_{(n)}^{fuzzy}\}$ *be the sequence of iterative approximations produced by the* FEWCVT *algorithm. Then it holds that for* $n = 1, 2, \ldots,$

$$E^{fuzzy}(\mathcal{W}_{(n)}, \mathcal{D}_{(n)}^{fuzzy}) \le E^{fuzzy}(\mathcal{W}_{(n-1)}, \mathcal{D}_{(n)}^{fuzzy}) \le E^{fuzzy}(\mathcal{W}_{(n-1)}, \mathcal{D}_{(n-1)}^{fuzzy}).$$

5. Experimental results

In this section, we will apply the FEWCVT segmentation on various synthetic and real images that are either clear of noise or corrupted by different types of noises and distortions. Furthermore, we will show the performance of the proposed FEWCVT algorithm by presenting visual and quantitative results and comparisons with eight well-known fuzzy clustering algorithms FCM_S, FCM_S1, FCM_S2, EnFCM, FGFCM, FGFCM_S1, FGFCM_S2, and FLICM. As mentioned in Section 1, some of these comparison fuzzy clustering algorithms, such as FCM_S, FCM_S1, FCM_S2, and FLICM, incorporate local spatial information using the regularization strategy, while others, such as FCM_S1, FCM_S2, EnFCM, and FGFCM, incorporate local spatial information using the image smoothing strategy.

We quantitatively evaluate the clustering results in terms of the segmentation accuracy (SA) and the F-measure, where SA is defined as follows [7]:

$$SA = \frac{Number\ of\ correctly\ classified\ pixels}{Total\ number\ of\ pixels}, \tag{32}$$

and F-measure is the harmonic mean of precision and recall, i.e.,

$$F = 2 \cdot \frac{Precision \cdot Recall}{Precision + Recall}. \tag{33}$$

There are totally four parameters that can be tuned in the FEWCVT algorithm:

- L, the number of clusters;
- λ, the weighting parameter that balances the clustering energy and the edge energy;
- ω, which defines the size of the local neighborhood $\mathbb{N}_\omega(\mathbf{p})$ (we take $\mathbb{N}_\omega(\mathbf{p})$ to be a square centered at $\mathbf{p}$);
- m, the weighting exponent on each fuzzy membership.

The settings of parameters L, λ, and ω are often depending on the content of the test image. We refer to [13,29,16] for detailed discussions on effect and determination of these parameters. Especially, without extra specification the weighting parameter λ in FEWCVT will be obtained by a searching for optimal value with respect to the F-measure for each image. As for the fuzziness parameter m, we will investigate its effect in this paper. It is worthy noting that $m = 2$ is a very common choice in most of the existing comparison algorithms.

Theoretically, the iterations of the FEWCVT algorithm proceed until the energy function stops changing, but in practical situation, this termination criterion does not need to be strictly satisfied, instead a termination criterion such as

$$\frac{E_{i+1} - E_i}{E_i} < \epsilon \tag{34}$$

could be used. This way can effectively reduce the running time. Furthermore, a maximum allowed iterations *maxIter* can also be set to stop the algorithm. In all the experiments, we set $\varepsilon = 10^{-3}$, $maxIter = 100$ in the termination criterion. We also would take the CVT clustering result as the initial configuration of the FEWCVT clustering, which substantially reduces the required iterations for FEWCVT convergence and leads to more stable results as shown for the EWCVT model in [13].

Fig. 1-left shows a simple clear synthetic image (with 3 different intensity clusters taken as 20, 120 and 220). Highly sharp and clean edges are rare in real images, there are often noises and intensity transition regions. In order to simulate these situations, we also modify the clear image by a Gaussian noise with $\sigma = 0.15$ and a Gaussian blurring (size $= 8$, $\sigma = 10$) respectively to get the corrupted ones that are given in Fig. 1-middle and Fig. 1-right. We specially note that $L = 2$ will not be able to handle this example no matter which clustering algorithm is used due to the intersection of three clusters in the images.

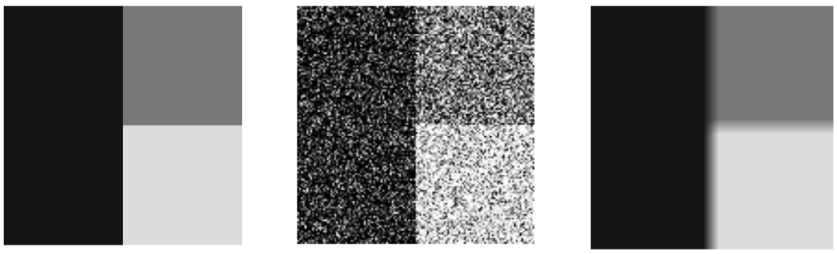

Fig. 1. A simple synthetic image and its corrupted versions. From left to right: the original clear image, the one corrupted by a Gaussian noise with $\sigma = 0.15$, and the one corrupted by a Gaussian blurring (size $= 8, \sigma = 10$).

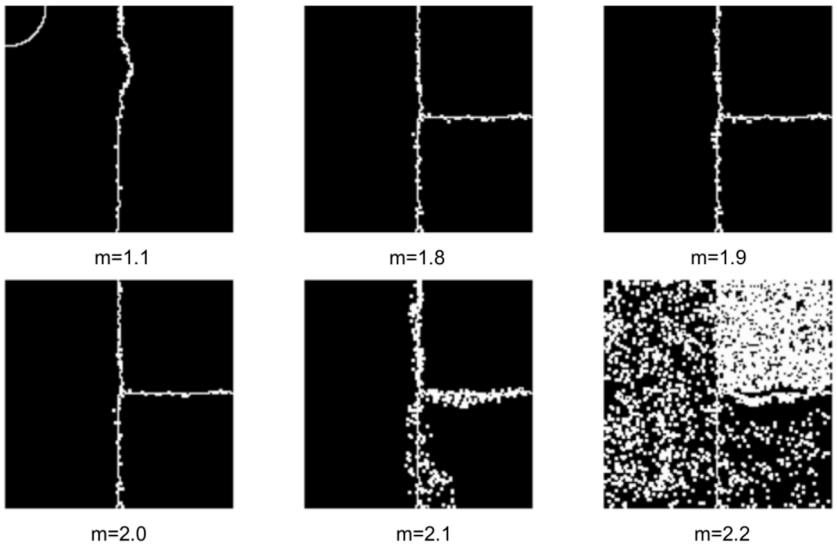

Fig. 2. Segmentation results of the synthetic noisy image of Fig. 1-middle by FEWCVT with different fuzziness parameter m.

We first investigate the effect of the fuzziness parameter m in the FEWCVT model by applying the FEWCVT algorithm with different fuzziness parameter m to the noisy image (Fig. 1-middle). We set $L = 3$ and $\omega = 6$ in the experiment. We tested the cases of $m = 1.1, 1.8, 1.9, 2.0, 2.1, 2.2$ and the segmentation results are visually illustrated in Fig. 2. From the experiments, we can see that smaller m leads to more information loss while larger m causes less effectiveness to noise removal. More specifically, the results with $m = 1.8, 1.9$ still look fine but that with $m = 2.1, 2.2$ are very poor and unacceptable, and overall $m = 2$ is the best choice that coincides with the existing fuzzy clustering algorithms. Therefore we set $m = 2$ in all the following experiments for all fuzzy clustering algorithms.

Next we compare the performance of FEWCVT with the eight popular fuzzy clustering algorithms by applying all of them to the three images in Fig. 1. We set the cluster number $L = 3$ and the neighborhood size $\omega = 6$ in all algorithms. In addition, the parameters that control the effect of local spatial information for the eight existing algorithms are also obtained by searching with respect to the optimal F-measure.

Fig. 3 presents the visual segmentation results of the clear image (Fig. 1-left) together with their SA and F-measure scores, in which the white lines represent the clustering boundaries. Because there is no noise at all in this image, the classic FCM can do perfect segmentation. It is easy to see from the figure that while FEWCVT, FCM_S2 and FGFCM_S2 perform almost perfectly, FCM_S, FCM_S1, EnFCM, FGFCM, FGFCM_S1 and FLICM all introduce a narrow segmentation gap in the segmentation results along the high-contrast image boundary between intensity values 20 and 220. We find that the segmentation gap is caused by the existence of another intermediate level cluster with a value of 120. Such cluster associated with the intermediate level centroid tends to be the best choice for the pixels along the high-contrast edges when applying the local spatial constraint based on the image intensity. We remark that this situation will not happen in two-cluster cases. FEWCVT can naturally avoid this clustering error because FEWCVT imposes a penalty on the length of cluster boundaries which is unrelated to image intensity. FCM S2 and FGFCM S2 also work well in this experiment, indicating that the use of median filtering could avoid the segmentation gap along the sharp edges.

Fig. 4 presents the segmentation results of the noisy image (Fig. 1-middle) together with their SA and F-measure scores. It can be seen that FEWCVT obviously outperforms its competitors. Besides the segmentation error due to noises, all comparison fuzzy algorithms introduce a narrow segmentation gap in the segmentation results along the high-contrast image boundary. In particular, FCM_S2 and FGFCM_S2 fail in this case, implying that the median filtering may not help

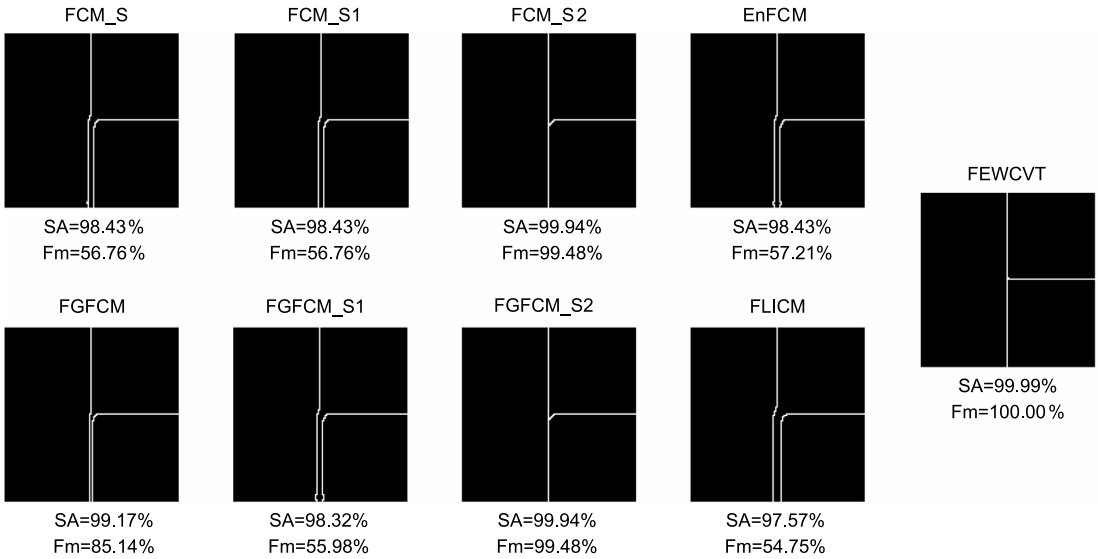

Fig. 3. Visual and quantitative results of segmentation of the synthetic clear image (Fig. 1-left) by different fuzzy clustering algorithms.

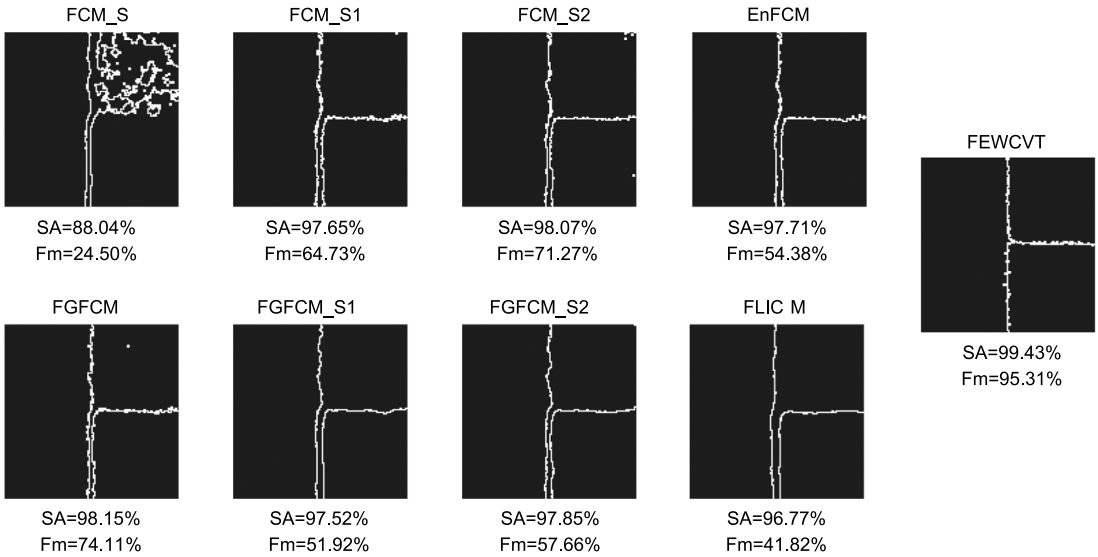

Fig. 4. Visual and quantitative results of segmentation of the synthetic noisy image (Fig. 1-middle) by different fuzzy clustering algorithms.

much on segmenting high-contrast but noisy boundaries when there are more than 2 clusters. Fig. 5 presents segmentation results of the blurred image (Fig. 1-right) using FEWCVT and the comparison fuzzy clustering algorithms. Again FEWCVT performs the best, and the segmentation gaps appear in all the comparison algorithms including FCM_S2 and FGFCM_S2.

Fig. 6 shows the segmentation results on more complicated synthetic images with more complex-shaped segments. Column 1 presents the original clear images and these images are then corrupted by Gaussian or Salt & Pepper noises with different levels (the noise levels are 5%, 15%, and 25%) to get noisy images in other columns. This experiment is a typical test used for evaluating previous fuzzy-clustering based segmentation methods in prior literature. In this experiment, ω is set to 3 and L is set from 2 to 7 respectively depending on each specific image. Table 1 lists the average F-measures (over all the cases of different cluster numbers) of the segmentation results for FEWCVT and the comparison algorithms. Fig. 7 shows the visual illustration of the results by FEWCVT. From these results, we can see that, FEWCVT overall works the best among all the tested algorithms. The proposed FEWCVT method shows excellent robustness to noises, and such robustness is relatively independent of the types of noises. Furthermore, FEWCVT works very well when using different cluster numbers.

Finally, Fig. 8 presents the FEWCVT segmentation results of several real images with two and three clusters, respectively. Although all five images in this experiment have serious inhomogeneous regions, the FEWCVT method can segment them very accurately.

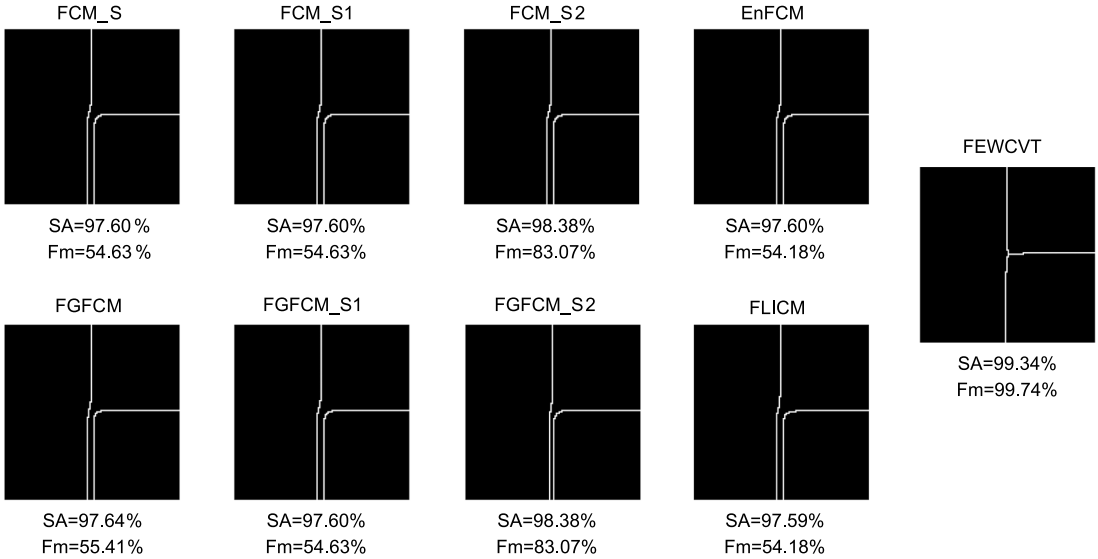

Fig. 5. Visual and quantitative results of segmentation of the synthetic blurred image (Fig. 1-right) by different fuzzy clustering algorithms.

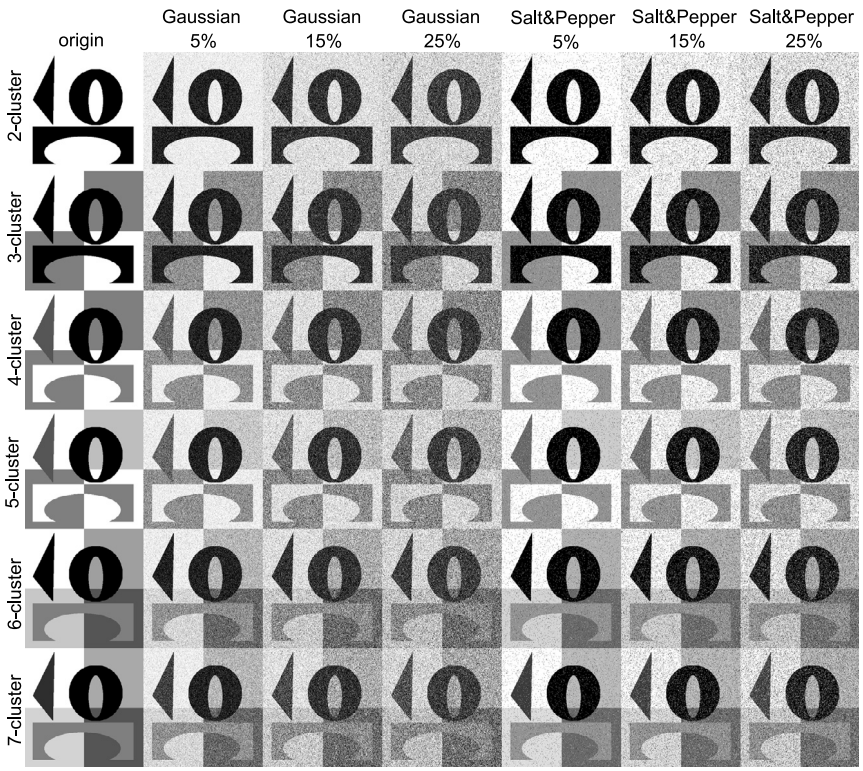

Fig. 6. A set of synthetic images of geometric shapes with different cluster numbers and the corresponding corrupted images with different levels of added noises (Gaussian or salt & pepper).

6. Conclusions

In this paper, we proposed a fuzzy edge-weighted centroidal Voronoi tessellation (FEWCVT) model for image segmentation and an iterative algorithm that minimizes the FEWCVT energy. Compared to existing fuzzy clustering algorithms that incorporate local spatial information, the proposed model instead introduces the fuzzy edge energy to the objective function, which can be viewed as an extension to the edge energy developed in EWCVT [13]. We also demonstrate

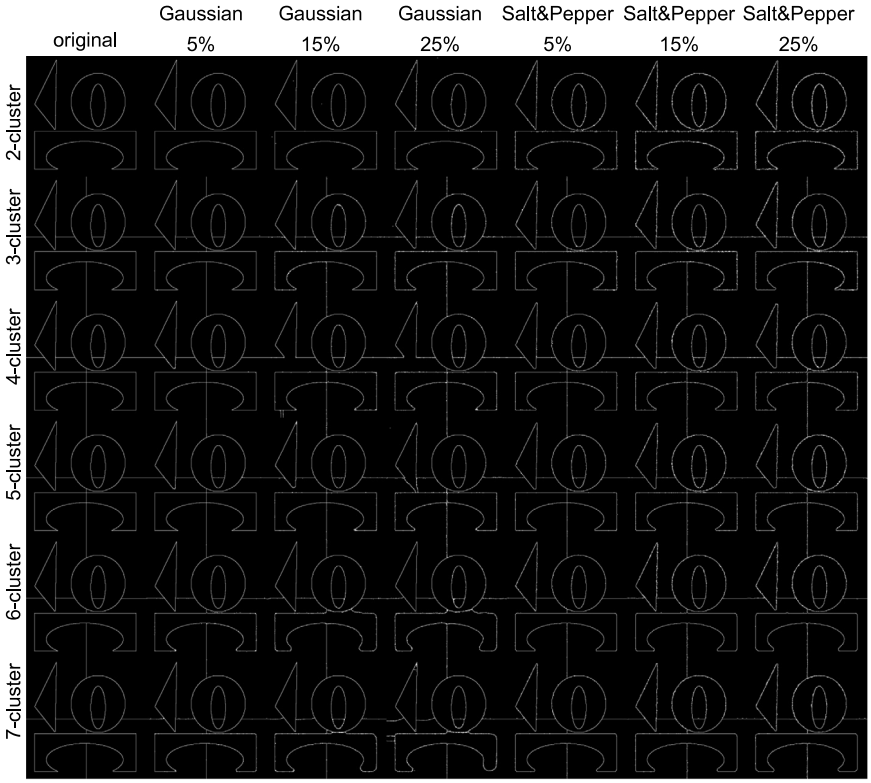

Fig. 7. FWECVT segmentation results of the synthetic images of geometric shapes shown in Fig. 6.

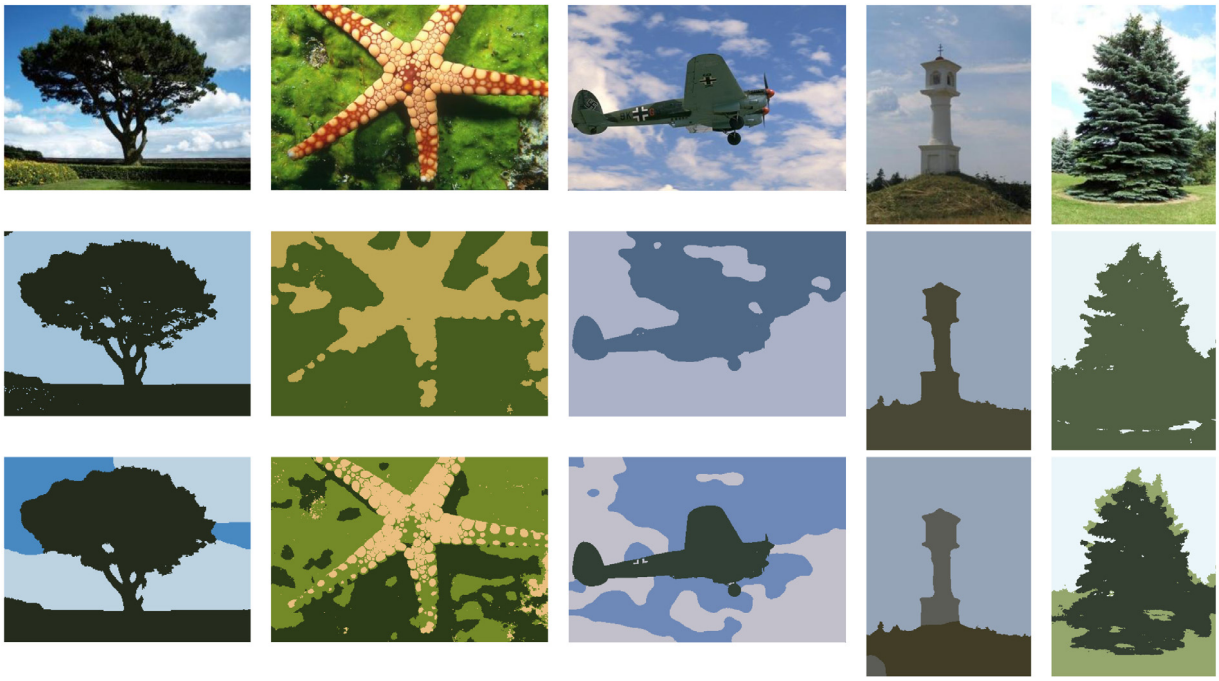

Fig. 8. Segmentation results of several real images using FEWCVT with $\lambda = 45\,000$. Top row: original images; middle row: segmented images by using 2 clusters ($L = 2$); bottom row: segmented images by using 3 clusters ($L = 3$).

the superior performance of FEWCVT through various experiments and comparisons with several popular fuzzy clustering algorithms.

Table 1
Average F-measures of the segmentation results of the images in Fig. 6 using different fuzzy clustering algorithms.

F-measure	FCM_S	FCM_S1	FCM_S2	EnFCM	FGFCM	FGFCM_S1	FGFCM_S2	FLICM	FEWCVT
5% Gauss	74.46%	88.15%	99.30%	82.54%	97.94%	79.71%	99.13%	79.04%	**99.58**%
15% Gauss	58.43%	78.94%	91.37%	76.72%	79.70%	76.84%	91.10%	78.18%	**99.16**%
25% Gauss	52.09%	74.10%	74.16%	65.66%	75.09%	74.67%	76.27%	77.95%	**97.90**%
5% Sa & Pe	59.70%	75.52%	**99.31**%	77.19%	94.45%	76.98%	98.88%	78.93%	98.99%
15% Sa & Pe	38.38%	48.04%	**99.37**%	51.18%	76.56%	60.05%	98.73%	69.87%	98.97%
25% Sa & Pe	37.85%	31.10%	**99.36**%	31.28%	48.73%	42.68%	99.14%	49.22%	98.84%

References

[1] L. Shapiro, G. Stockman, Computer Vision, Prentice Hall, 2001.
[2] J. Hartigan, Clustering Algorithms, John Wiley & Sons, Inc., 1975.
[3] S. Nascimento, B. Mirkin, F. Moura-Pires, A fuzzy clustering model of data and fuzzy c-means, in: Proc. IEEE Inter. Conf. Fuzzy Syst., Vol. 1, 2000, pp. 302–307.
[4] J. Bezdek, Pattern Recognition with Fuzzy Objective Function Algorithms, Kluwer Academic Publishers, 1981.
[5] L. Szilagyi, Z. Benyo, S. Szilagyi, H. Adam, MR brain image segmentation using an enhanced fuzzy C-means algorithm, in: Proc. IEEE Inter. Conf. EMBS, 2003, pp. 17–21.
[6] W. Cai, S. Chen, D. Zhang, Fast and robust fuzzy C-means clustering algorithms incorporating local information for image segmentation, Pattern Recognit. 40 (2007) 825–838.
[7] M. Ahmed, S. Yamany, N. Mohamed, A. Farag, T. Moriarty, A modified fuzzy C-means algorithm for bias field estimation and segmentation of MRI data, IEEE Trans. Med. Imaging 21 (2002) 193–199.
[8] S. Chen, D. Zhang, An adaptive fuzzy C-means algorithm for image segmentation in the presence of intensity inhomogeneities, IEEE Trans. Syst. Man Cybern. 34 (2004) 1907–1916.
[9] S. Krinidis, V. Chatzis, A robust fuzzy local information C-means clustering algorithm, IEEE Trans. Image Process. 19 (2010) 1328–1337.
[10] T. Chan, L. Vese, An efficient variational multiphase motion for the Mumford–Shah segmentation model, in: Proc. Asilomar Conf. Signals Syst. Comput., Vol. 1, 2000, pp. 490–494.
[11] T. Chan, L. Vese, Active contours without edges, IEEE Trans. Image Process. 10 (2001) 266–277.
[12] T. Chan, L. Vese, Active contour and segmentation models using geometric PDE's for medical imaging, in: R. Malladi (Ed.), Geometric Methods in Bio-Medical Image Processing, Springer, Berlin, Germany, 2002, pp. 63–75.
[13] J. Wang, L. Ju, X. Wang, An edge-weighted centroidal Voronoi tessellation model for image segmentation, IEEE Trans. Image Process. 18 (2009) 1844–1858.
[14] Y. Cao, L. Ju, Q. Zou, C. Qu, S. Wang, A multichannel edge-weighted centroid Voronoi tessellation algorithm for 3D superalloy image segmentation, in: Proc. IEEE Conf. Comput. Vision Pattern Recognition, 2011, pp. 17–24.
[15] Y. Cao, L. Ju, S. Wang, Grain segmentation of 3D superalloy images using multichannel EWCVT under human annotation constrains, in: Procs. Euro. Conf. Comput. Vision, 2012, pp. 244–257.
[16] J. Wang, L. Ju, X. Wang, Image segmentation using local variation and edge-weighted centroidal Voronoi tessellations, IEEE Trans. Image Process. 20 (2011) 3242–3256.
[17] J. Wang, X. Wang, VCells: simple and efficient superpixels using edge-weighted centroidal voronoi tessellations, IEEE Trans. Pattern Anal. Mach. Intell. 34 (2012) 1241–1247.
[18] Q. Du, V. Faber, M. Gunzburger, Centroidal Voronoi tessellations: applications and algorithms, SIAM Rev. 41 (1999) 637–676.
[19] Q. Du, M. Gunzburger, L. Ju, Constrained centroidal Voronoi tessellations for surfaces, SIAM J. Sci. Comput. 24 (2003) 1488–1506.
[20] Q. Du, M. Gunzburger, L. Ju, X. Wang, Centroidal Voronoi tessellation algorithms for image compression, segmentation, and multichannel restoration, J. Math. Imaging Vision 24 (2006) 177–194.
[21] A. Hausner, Simulating decorative mosaics, in: Proc. Conf. Comput. Graph. Interact. Tech., 2001, pp. 573–580.
[22] L. Ju, Q. Du, M. Gunzburger, Probabilistic methods for centroidal Voronoi tessellations and their parallel implementations, Parallel Comput. 28 (2002) 1477–1500.
[23] T. Kanungo, D. Mount, N. Netanyahu, C. Piatko, R. Silverman, A. Wu, An efficient k-means clustering algorithm: Analysis and implementation, IEEE Trans. Pattern Anal. Mach. Intell. 24 (2002) 881–892.
[24] J. Hartigan, M. Wong, A k-means clustering algorithm, J. Roy. Statist. Soc. Ser. C 28 (1979) 100–108.
[25] D. Sparks, Euclidean cluster analysis, J. Roy. Statist. Soc. Ser. C 22 (1973) 126–130.
[26] H. Spath, Cluster Dissection and Analysis Theory: FORTRAN Programs, Examples, Prentice Hall, 1985.
[27] D. Bertsekas, Nonlinear Programming, Athena Scientific, 1981.
[28] W. Wang, M.A. Carreira-Perpinán, Projection onto the probability simplex: an efficient algorithm with a simple proof, and an application, 2013. arXiv:1309.1541.
[29] J. Liu, X. Tai, H. Huang, Z. Huan, A fast segmentation method based on constraint optimization and its applications: Intensity inhomogeneity and texture segmentation, Pattern Recognit. 44 (2011) 2093–2108.